




Superconductivity at 12 K in La_2IOs_2 : A $5d$ metal with osmium honeycomb layerHajime Ishikawa ^{*}, Takeshi Yajima , Daisuke Nishio-Hamane, Shusaku Imajo , and Koichi Kindo
*Institute for Solid State Physics, University of Tokyo, Kashiwa, Chiba 277-8581, Japan*Mitsuaki Kawamura *Information Technology Center, University of Tokyo, Bunkyo-ku, Tokyo 113-8658, Japan*

(Received 17 February 2023; accepted 16 May 2023; published 31 May 2023)

We discovered superconductivity at $T_c = 12$ K in a layered compound La_2IOs_2 with an osmium honeycomb network. Despite heavy constituent elements unfavorable for a phonon mediated mechanism, T_c is the highest among lanthanoid iodides made of lighter elements such as La_2IRu_2 with $T_c = 4.8$ K. Electronic anomalies are observed below 60 K similar to those observed in La_2IRu_2 below 140 K. La_2IOs_2 is a layered $5d$ electron system providing a platform to investigate the interplay between the electronic anomaly, superconductivity, and strong magnetic field.

DOI: [10.1103/PhysRevMaterials.7.054804](https://doi.org/10.1103/PhysRevMaterials.7.054804)**I. INTRODUCTION**

$4d$ and $5d$ transition metal compounds have gained considerable interest in the condensed matter community. The combination of strong spin-orbit coupling and Coulomb interactions may stabilize a Mott insulating state with nontrivial ground states such as a quantum spin liquid and multipolar orders [1]. In metallic compounds, the spin-orbit coupling and electron-electron interactions may cause a Fermi surface instability that gives rise to various electronic orders [2].

Realizations of exotic superconductivity have been discussed in $5d$ transition metal compounds. Carrier doping on the spin-orbit coupled Mott insulator such as layered iridate is a possible avenue [3–6]. In SrPtAs with an ordered honeycomb layer made of platinum and arsenide, an unusual Cooper pairing state that breaks the time reversal symmetry is proposed [7–9]. Pyrochlore oxide superconductor $\text{Cd}_2\text{Re}_2\text{O}_7$ exhibits a phase transition at 200 K below which the space inversion symmetry is broken [10,11]. Odd-parity superconductivity is proposed to appear at the vicinity of the inversion breaking order [12,13].

In 2019, a peculiar layered superconductor La_2IRu_2 with $T_c = 4.8$ K was reported [14] which crystallizes in the Gd_2IFe_2 -type known as the intermediate between cluster compounds and intermetallic phases [15]. The crystal structure features a two-dimensional slab made of a transition-metal-centered trigonal prism of lanthanoid, where transition metals form the honeycomb network [Fig. 1(a)]. The slabs are separated by iodine anions. The first-principles calculation revealed the dominant contributions of Ru- $4d$ and La- $5d$ orbitals at the Fermi level. The calculated effective valence for ruthenium was close to -1 based on the Bader charge analysis [16], i.e., the ruthenium is anionic in contrast to cations in honeycomb Mott insulators such as α - RuCl_3 [17], Li_2RuO_3

[18], and SrRu_2O_6 [19] with valences of $+3$, $+4$, and $+5$, respectively. Superconductivity in La_2IRu_2 violates the Pauli limit expected for the spin-singlet superconductor. Preceding the superconductivity, anomalies are observed in the magnetic susceptibility and the electrical resistivity with small structural changes below 140 K. These observations suggest La_2IRu_2 is a layered superconductor made of heavy elements with uncommon electronic states. Little is known about the superconductivity, including the universality in the isostructural compounds, the pairing mechanism, and the roles of the spin-orbit coupling of the $4d$ and $5d$ electrons. Here, we synthesized La_2IOs_2 [20], where $5d$ Os replaces the $4d$ Ru in La_2IRu_2 , and investigated its physical properties. We discovered superconductivity at 12 K preceded by the electronic and structural anomalies below 60 K.

II. SAMPLE PREPARATION

A powder sample of La_2IOs_2 was synthesized by a solid state reaction from the powders of LaI_3 , La (99.9%), and Os (99.9%). LaI_3 was synthesized by reacting small pieces of La and iodine (99.999%) with a molar ratio of 1:4 at 950°C for 12 h inside an evacuated quartz glass tube. Excess iodine was removed by sublimation after the reaction. La powder was prepared by filing a rod of La metal. LaI_3 , La, and Os were weighed with the molar ratio of 1:5:6 and mixed in an agate mortar. The powder was sealed inside a tantalum tube and was further sealed inside an evacuated quartz glass tube. The tube was heated at 900°C for 6 days. The reaction yields a dark gray powder. Note that all the experimental procedures were performed inside an argon-filled glove box because the starting and target materials are air and moisture sensitive, and Os may produce toxic oxides when exposed to air. To obtain single crystals, a similar reaction was performed in more inhomogeneous conditions by using small pieces of La instead of the powder as a starting material. The starting materials were sealed as described above and reacted at 950°C for 1 day and

^{*}hishikawa@issp.u-tokyo.ac.jp

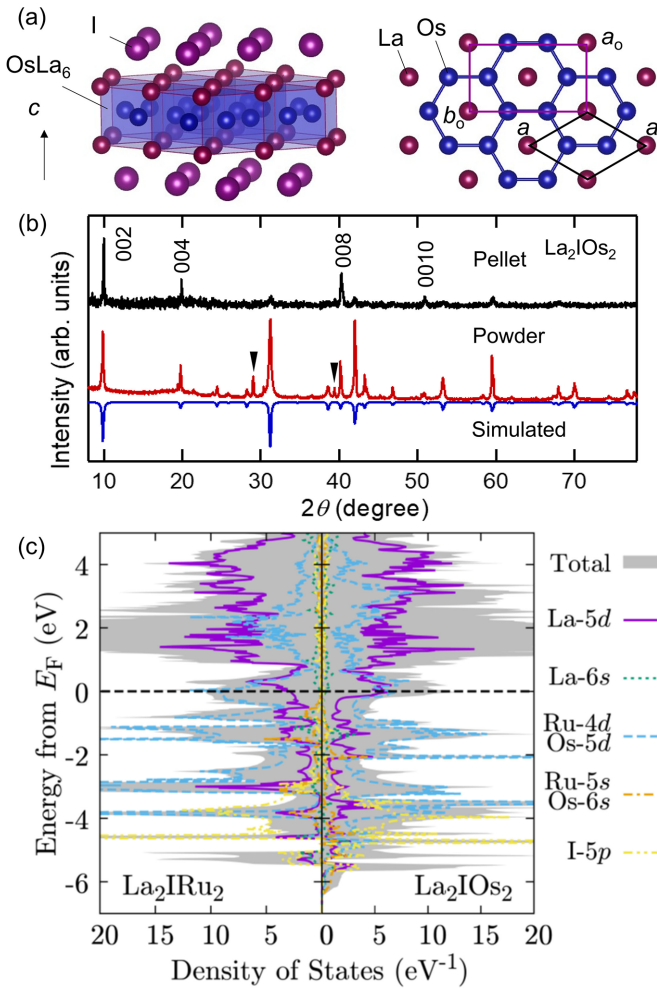


FIG. 1. Crystal structure of La_2IOs_2 seen from the in-plane direction (left) and from the c axis (right) described by VESTA [21]. Hexagonal and orthorhombic unit cells are shown by the black and purple lines, respectively. (b) X-ray diffraction patterns of powder (middle) and a pellet (top) of La_2IOs_2 compared with the calculated pattern (bottom). Triangles indicate the LaOI impurity phase. (c) Orbital projected density of states calculated on La_2IRu_2 (left) and La_2IOs_2 (right).

annealed at 900 °C for 6 days. The reaction yields inhomogeneous solids including small hexagonal platelet crystals [22].

Powder x-ray diffraction measurements were performed by a diffractometer with Cu- $K\alpha$ radiation (Smart Lab, Rigaku). The diffraction pattern was analyzed using the FULLPROF software [23]. The main peaks observed in the powder pattern shown in Fig. 1(b) match the simulated pattern of the Gd_2IFe_2 -type structure with the space group $P6_3/mmc$ and lattice constants $a = 4.2995(1)$ Å and $c = 17.953(1)$ Å at 300 K, which are close to the values in the previous report [20]. Extra peaks can be attributed to the small amount of LaOI impurity phase. LaOI with La^{3+} ($4f^0$) ion does not possess active electrons and can be negligible in the physical properties measurements. Chemical analysis of the hexagonal crystals used for the torque measurements were performed using scanning electron microscopy (SEM, JEOL IT-100) equipped with energy dispersive X-ray spectroscopy (EDS,

15 kV, 0.8 nA), which revealed a chemical composition close to La_2IOs_2 [22].

III. EXPERIMENTAL METHODS

Electrical resistivity measurements were performed by the four-terminal method using the commercial apparatus (PPMS, Quantum Design). A thin plate-shaped pellet is made by pressing the powder sample and used for the measurements. The powder x-ray diffraction pattern for the pellet mounted parallel to the sample holder exhibits predominantly (00 l) diffraction peaks as in Fig. 1(b), indicating sizable preferred orientation along the c axis. Au wires were attached on the pellet by silver paint. To prevent the degradation of the sample in air at the sample installation for measurements, the whole sample was covered by an epoxy resin after the wiring. Magnetization measurements of the powder sample at 2–300 K and at 0–6 T were performed by a SQUID magnetometer (MPMS-XL, Quantum Design). The powder was sealed inside a plastic tube or Al foil and the corresponding background signal was subtracted. Specific heat measurements were performed by the relaxation method using a commercial apparatus (PPMS, Quantum Design). A small piece of the powder pellet was attached to the sample stage by the apiezon-N grease. Magnetic torque was measured by a microcantilever technique. A hexagonal plate-shaped crystal with approximately 100 μm size was picked up inside the Ar-filled glove box. The crystal was covered by the apiezon-N grease and attached to the microcantilevers [22], which can be rotated in the magnetic field. The magnetic torque of the crystal was measured as the change in the resistance of the microcantilever.

IV. CALCULATION METHODS

The electronic states of La_2IOs_2 and La_2IRu_2 were investigated by the first-principles electronic-structure calculation based on density functional theory. We employed the plane-waves and pseudopotentials-based program package QUANTUM ESPRESSO [24]. Perdew-Burke-Ernzerhof's density functional [25] based on generalized gradient approximation (GGA) was used. To represent the wave function and the atomic potential, we set the cutoff energy to 80 Ry and used fully relativistic optimized norm-conserving pseudopotential [26] since we include the spin-orbit interaction in the calculation. The Brillouin-zone integration in the calculation of charge density (density of states) was performed on a $10 \times 10 \times 2$ ($20 \times 20 \times 4$) \mathbf{k} -point grid using the optimized tetrahedron method [27]. To analyze the contribution from each atom, we computed the projected density of states by projecting each Kohn-Sham state onto atomic orbitals used in the generation of pseudopotentials. Bader charge analysis [16] was performed using a code provided by the Henkelman group [28] together. For this analysis, we employed a projector augmented wave [29] data set in PSLIBRARY [30] with a cutoff energy of 75 Ry. The calculated orbital projected density of state is shown in Fig. 1(c). The band dispersion is shown in the Supplemental Material [22].

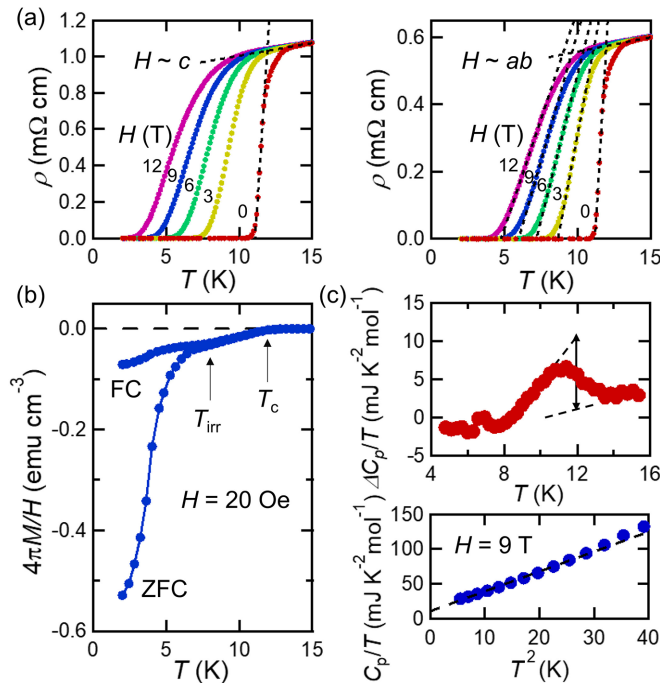


FIG. 2. (a) Temperature dependences of electrical resistivity in the magnetic field perpendicular (left) and parallel (right) to the pellet: different pellets from the same powder sample are used. (b) Temperature dependence of $4\pi M/H$ of the powder sample of La_2IOs_2 at $H = 20$ Oe. (c) Difference of the specific heat divided by temperature between the 0 and 9 T data (top): the dashed lines and the arrow are the eye guide. 9 T data is plotted against T^2 (bottom).

V. RESULTS

Electrical resistivity $\rho(T)$ measured on the powder pellet is shown in Fig. 2(a). At zero magnetic field, the $\rho(T)$ decreases linearly below 20 K and deviates downward below 13 K. The zero resistance is observed at 11 K, indicating a superconducting transition. The linear extrapolations of the $\rho(T)$ above 13 K and the fit in the temperature range where ρ steeply decreases cross at 12 K, providing an estimation of $T_c = 12$ K. The decrease in ρ above T_c may be attributed to the superconducting fluctuations or a certain inhomogeneity in the sample.

To check the Meissner effect, we measured magnetization M on the powder sample in a weak magnetic field [Fig. 2(b)]. After zero field cooling (ZFC), the large diamagnetic signal is observed. In the magnetic field at $H = 20$ Oe, $4\pi M/H$, which corresponds to the superconducting volume fraction, is larger than 50% at 2 K, suggesting bulk superconductivity. M/H increases rapidly as increasing temperature up to around 8 K and gradually increases up to around 12 K. On field cooling (FC), the M/H takes slightly larger values than in the ZFC process, down to around 8 K, and a clear ZFC-FC hysteresis is observed below 8 K.

At first glance, the M/H appears to be that of the powder containing two superconducting phases with T_c of 8 and 12 K. However, the absence of clear ZFC-FC hysteresis just below T_c and the appearance of the hysteresis at lower temperature are often observed in layered superconductors with weak vortex pinning, including high- T_c cuprate [31] and Li_xHfNCI

[32,33]. The temperature where the hysteresis appears is called the irreversibility temperature T_{irr} , above which vortices are free to move. The behavior of M/H suggests La_2IOs_2 is a superconductor with $T_c = 12$ K and $T_{\text{irr}} = 8$ K.

To confirm bulk superconductivity at 12 K, we measured the temperature dependence of specific heat C_p on a thin plate-shaped powder pellet with preferred orientation along the c axis [Fig. 1(c)]. Large lattice contribution around T_c makes the accurate analysis of the electronic contribution challenging. Nevertheless, a peak is observed when the C_p/T data at 9 T applied perpendicular to the pellet is subtracted from the 0 T data [Fig. 2(c)]. The peak appears at around 12 K but not around 8 K, supporting the bulk superconductivity at 12 K. The estimated jump of the C_p/T at 12 K is approximately 10 mJ/mol K². C_p/T at 9 T is plotted against T^2 and the low-temperature data is linearly fitted assuming $C_p = \gamma T + \beta T^3$, where the first and second terms indicate the electronic and lattice specific heat, respectively. The fit yields $\gamma = 11(1)$ mJ/mol K² and $\beta = 2.85(6)$ mJ/mol K⁴. The Debye temperature calculated from β is 150 K. The estimated $\Delta C_p/\gamma T_c$ is 0.91, which is smaller than 1.43 for the full gap superconductor. Note that the superconductivity is not fully suppressed at 9 T, as discussed later, and the quantitative discussion is hard based on the present data.

The effect of the magnetic field is examined by measuring $\rho(T)$ in the magnetic field applied parallel and perpendicular to the pellet, which can mimic the $H // ab$ and c conditions, respectively [Fig. 2(a)]. The drop of resistivity is suppressed toward low temperatures in both field directions. The effect of the magnetic field is weak in H parallel to the pellet, which is consistent with the expectation that the orbital pair breaking effect is suppressed when the magnetic field is applied parallel to the superconducting layer. The superconducting transition survives in a relatively strong magnetic field at 12 K.

To estimate the upper critical field in $H // ab$ more precisely, we measured the magnetic torque τ on a small single crystal [Fig. 3(a)]. In a layered superconductor, the Meissner diamagnetic moment tends to orient perpendicular to the layer because the superconducting current may flow more easily within the layer. As τ is proportional to $\mathbf{M} \times \mathbf{H}$, the torque signal is nearly zero at $H // c$, while a large signal is observed near $H // ab$. In the magnetic field angle dependence of τ , a sharp anomaly is expected across $H // ab$, where the τ changes the sign: the rotation angle $\theta = 90^\circ$ corresponds to $H // ab$ in our data. Indeed, we observed a sharp anomaly at $\theta = 90^\circ$ at 4 K in $H = 6$ and 12 T. At elevated temperatures, the anomaly becomes broader and smaller but visible up to around 10.8 and 9.6 K at 6 and 12 T, respectively. Note that the magnetic torque of the single crystal is insensitive to the impurities on the surface of the crystal because they typically do not exhibit anisotropy. The observation of the clear torque signal evidences the bulk superconductivity.

The H - T phase diagram in $H // ab$ is obtained assuming the temperature where the anomaly of τ is barely visible as T_c . The temperature is slightly higher than T_c estimated from the linear interpolations of the $\rho(T)$ data on the powder pellet as described above [Fig. 3(a)] likely because the powder averaging is avoided and/or τ is sensitive to the superconducting fluctuations [34]. The linear fit for the T_c at 6 and 12 T estimated from the τ data and $T_c = 12$ K at 0 T yields a slope of

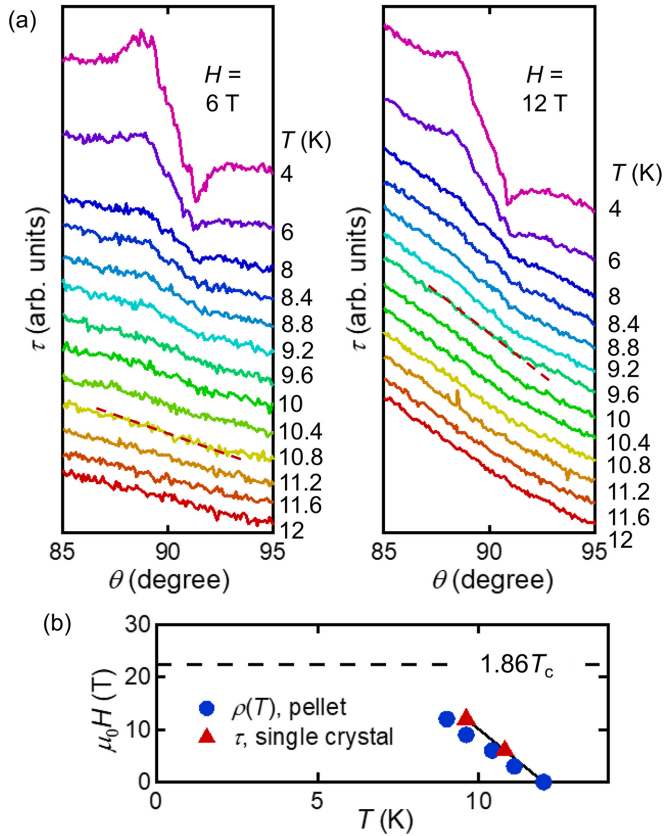


FIG. 3. Temperature and magnetic field angle dependence of the magnetic torque of a single crystal of La_2IOs_2 at 6 (left) and 12 (right) T. The dashed lines are the eye guide. (b) H - T phase diagram determined by the resistivity and torque data.

the H - T diagram $dH/dT = -5$ T/K. The orbital pair breaking field can be estimated by the Werthamer-Helfand-Hohenberg (WHH) theory as approximately $0.7 \times |dH/dT|_{T=T_c} \times T_c$ [35]. The estimation yields 42 T, which is larger than the Pauli limit of $1.86T_c = 22.3$ T. The violation of the Pauli limit is expected in La_2IOs_2 as in La_2IRu_2 [14].

In La_2IRu_2 , successive anomalies are observed in the magnetic susceptibility and electrical resistivity at around 140 and 85 K [14]. In La_2IOs_2 , we observed decreases in magnetic susceptibility at 60 and 30 K [Fig. 4(a)], which bear a resemblance to those observed in La_2IRu_2 . We call the temperatures of the high- and low-temperature anomalies T_{a1} and T_{a2} , respectively, following those in La_2IRu_2 . At T_{a1} , a clear kink is observed in $\rho(T)$. The anomaly at T_{a2} in $\rho(T)$ is weak, but there appears a weak change of the slope.

We performed powder x-ray diffraction measurements at low temperature on La_2IOs_2 to examine possible structural changes at T_{a1} and T_{a2} . In the powder pattern, the splitting or broadening of the peaks are observed below 60 K [Fig. 4(b)], indicating the lowering of the crystal symmetry. The low-temperature data is analyzed assuming the orthorhombic unit cell [Fig. 1(a)]. The a -axis length in the orthorhombic unit cell (a_0) is the same with the hexagonal unit cell, while the b -axis length (b_0) corresponds to $\sqrt{3}a$ of the hexagonal unit cell. The temperature dependence of the refined lattice constants are plotted in Fig. 4(b): $b_0/\sqrt{3}$ is plotted to compare with

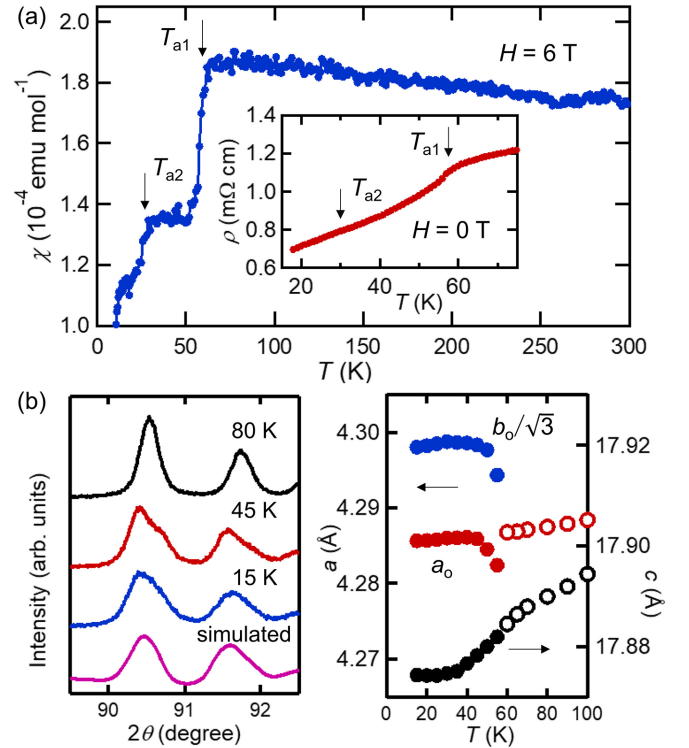


FIG. 4. (a) Temperature dependence of the magnetic susceptibility at 6 T of the powder sample of La_2IOs_2 . Electrical resistivity at 0 T is shown in the inset. (b) Powder x-ray diffraction pattern of La_2IOs_2 at selected temperatures compared with the simulation assuming the orthorhombic unit cell (left). Temperature dependence of the lattice constant of La_2IOs_2 (right): values for hexagonal and orthorhombic unit cells are shown by the open and filled plots, respectively.

a in the hexagonal cell. The average of the a_0 and $b_0/\sqrt{3}$ increases below 60 K, while the c axis shrinks. In the case of La_2IRu_2 , the a -axis length decreases but the c -axis length slightly increases below T_{a1} [14]. a_0 and b_0 in La_2IOs_2 slightly decrease below 30 K, while the changes are small.

VI. DISCUSSION

$T_c = 12$ K in La_2IOs_2 is the highest among layered lanthanoid iodides with related crystal structures. Thus far the highest observed T_c was 10 K in the iodide carbide $\text{Y}_2\text{I}_2\text{C}_2$ [36]. In $\text{La}_2\text{I}_2\text{C}_2$, superconductivity is observed below 2 K [37]. In La_2TeI_2 , where Te replaces the C_2 units, superconductivity is not reported [38]. Suppression of T_c on substituting $\text{Y}_2\text{I}_2\text{C}_2$ by heavier elements appears compatible with a phonon mediated superconductivity, where lighter elements that enhance the phonon frequencies are favored. We expect lower T_c in heavier La_2IOs_2 than in La_2IRu_2 : the Debye temperatures estimated from the specific heat measurements are 150 and 162 K in La_2IOs_2 and La_2IRu_2 , respectively. Contrary to the expectation, T_c of La_2IOs_2 is 2.5 times higher than La_2IRu_2 . The electronic specific heat coefficient γ is estimated as 11 and 13 mJ/mol K^2 on La_2IOs_2 and La_2IRu_2 , respectively. Smaller γ in La_2IOs_2 suggests the smaller density of states and is again opposed to the higher T_c .

La_2IOs_2 and La_2IRu_2 are distinguished from the $\text{Y}_2\text{I}_2\text{C}_2$ family by the presence of the high-temperature anomalies preceding the superconductivity at T_{a1} and T_{a2} , where similar decreases in the magnetic susceptibility are observed. The two compounds are made of the same group elements with similar effective valences verified by the Bader charge calculation: +1.41 (+1.37) for La, -0.80 (-0.79) for I, and -1.01 (-0.98) for Os (Ru) in La_2IOs_2 (La_2IRu_2). It would be reasonable to consider that the anomalies in the two compounds share a common origin. Enhancement of T_c upon suppression of an electronic order is observed in various layered superconductors including cuprates, iron pnictides, and charge-density-wave systems [39–43]. The relationship between the high-temperature anomalies and T_c in La_2IOs_2 and La_2IRu_2 follows this trend, pointing to an interplay between the high-temperature anomalies and the superconductivity.

The drop of magnetic susceptibility at T_{a1} and T_{a2} should indicate a decrease in the density of states at the Fermi energy or an antiferromagnetic order. Antiferromagnetic order is not compatible with the results of nuclear magnetic resonance experiments on La_2IRu_2 [14]. More delocalized $5d$ orbitals in La_2IOs_2 should further destabilize the magnetism [22]. A charge-density-wave order can be compatible with the observations. The decrease in resistivity with a kink is similar to that observed at the charge-density-wave order in layered superconductors [41–43]. Note that there is one transition above the superconductivity in these charge-density-wave systems, in contrast to the two transitions observed in La_2IOs_2 and La_2IRu_2 .

We propose another possibility by pointing out the striking similarities between La_2IOs_2 and $5d$ pyrochlore superconductor $\text{Cd}_2\text{Re}_2\text{O}_7$ [10]. $\text{Cd}_2\text{Re}_2\text{O}_7$ exhibits successive phase transitions at 200 and 120 K accompanying the decreases in magnetic susceptibility and resistivity similar to La_2IOs_2 . Suppression of the transitions by applying pressure raises the T_c and enhances the upper critical field above the Pauli limit [44]. $\text{Cd}_2\text{Re}_2\text{O}_7$ gains attention as the spin-orbit coupled metal, where an interplay between an electronic order and the odd-parity superconductivity is proposed [2, 11–13]. As seen in the orbital projected density of states [Fig. 1(c)], the bands around the Fermi energy are dominated by the Os- $5d$ and La- $5d$ orbitals, where a strong effect of spin-orbit coupling is expected. Examining whether the high-temperature anomalies and the superconductivity with high upper critical field are relevant to those discussed in the spin-orbit coupled system would be an intriguing problem.

In addition to the suppressed high-temperature anomalies, the difference in the lattice distortions at low temperature may play a role in the enhancement of T_c in La_2IOs_2 compared to La_2IRu_2 . The single-crystal structural analysis on La_2IRu_2 points to the small displacement of Ru atoms along the c axis without clear symmetry lowering [14]. On the other hand, the powder x-ray diffraction on La_2IOs_2 suggests the in-plane distortions. The different lattice distortions observed in La_2IOs_2 and La_2IRu_2 may indicate different ordering patterns are energetically degenerate. The band structure calculations on the high-temperature hexagonal structure revealed the presence of several bands crossing the Fermi energy in both compounds [22]. The multiband superconductor may exhibit enhanced T_c [45], as extensively investigated in MgB_2 with $T_c = 39$ K [46], and high upper critical field, violating the Pauli limit as in the Chevrel phases with $T_c \sim 15$ K [47]. The band structure of La_2IOs_2 and La_2IRu_2 should be modified in different ways at low temperature. A certain multiband effect that enhances T_c may exist in the low-temperature band structure of La_2IOs_2 .

VII. CONCLUSION AND PERSPECTIVE

We discovered superconductivity at $T_c = 12$ K in a layered compound La_2IOs_2 . Successive anomalies are observed in the electronic properties below 60 K accompanying structural changes. The superconductivity is suppressed only by a few kelvins in magnetic field at 12 T. La_2IOs_2 is a $5d$ electron system that allows us to investigate the interplay between electronic anomalies, superconductivity, and high magnetic field in a layered structure featuring honeycomb lattice. Further investigations to clarify the nature of the high-temperature anomalies and its relationship to superconductivity are necessary. If the corresponding order promotes superconductivity, higher T_c can be obtained around the quantum critical point, providing a so-called superconducting dome in the phase diagram. Examining the evolution of T_{a1} , T_{a2} , and T_c against a certain control parameter by performing doping or high-pressure experiments is desired. Uncovering the H - T phase diagram at the high magnetic field region would be informative for discussing the multiband effect.

ACKNOWLEDGMENTS

We would like to thank Prof. Zenji Hiroi and Prof. Yoshihiko Okamoto for help in the use of osmium and fruitful discussions. H.I. is supported by JSPS KAKENHI Grants No. JP22H04467 and No. JP22K13996.

-
- [1] W. Witczak-Krempa, G. Chen, Y. B. Kim, and L. Balents, *Annu. Rev. Condens. Matter Phys.* **5**, 57 (2014).
 - [2] L. Fu, *Phys. Rev. Lett.* **115**, 026401 (2015).
 - [3] Y.-Z. You, I. Kimchi, and A. Vishwanath, *Phys. Rev. B* **86**, 085145 (2012).
 - [4] T. Hyart, A. R. Wright, G. Khaliullin, and B. Rosenow, *Phys. Rev. B* **85**, 140510(R) (2012).
 - [5] H. Watanabe, T. Shirakawa, and S. Yunoki, *Phys. Rev. Lett.* **110**, 027002 (2013).
 - [6] Z. Y. Meng, Y. B. Kim, and H.-Y. Kee, *Phys. Rev. Lett.* **113**, 177003 (2014).
 - [7] Y. Nishikubo, K. Kudo, and M. Nohara, *J. Phys. Soc. Jpn.* **80**, 055002 (2011).
 - [8] M. H. Fischer, T. Neupert, C. Platt, A. P. Schnyder, W. Hanke, J. Goryo, R. Thomale, and M. Sgrist, *Phys. Rev. B* **89**, 020509(R) (2014).
 - [9] P. K. Biswas, H. Luetkens, T. Neupert, T. Sturzer, C. Baines, G. Pascua, A. P. Schnyder, M. H. Fischer, J. Goryo, M. R. Lees,

- H. Maeter, F. Bruckner, H. H. Klauss, M. Nicklas, P. J. Baker, A. D. Hillier, M. Sigrist, A. Amato, and D. Johrendt, *Phys. Rev. B* **87**, 180503(R) (2013).
- [10] M. Hanawa, Y. Muraoka, T. Tayama, T. Sakakibara, J. Yamaura, and Z. Hiroi, *Phys. Rev. Lett.* **87**, 187001 (2001).
- [11] Z. Hiroi, J.-i. Yamaura, T. C. Kobayashi, Y. Matsubayashi, and D. Hirai, *J. Phys. Soc. Jpn.* **87**, 024702 (2018).
- [12] V. Kozii and L. Fu, *Phys. Rev. Lett.* **115**, 207002 (2015).
- [13] Y. Wang, G. Y. Cho, T. L. Hughes, and E. Fradkin, *Phys. Rev. B* **93**, 134512 (2016).
- [14] H. Ishikawa, U. Wedig, J. Nuss, R. K. Kremer, R. Dinnebie, M. Blankenhorn, M. Pakdaman, Y. Matsumoto, T. Takayama, K. Kitagawa *et al.*, *Inorg. Chem.* **58**, 12888 (2019).
- [15] M. Ruck and A. Simon, *Z. Anorg. Allg. Chem.* **619**, 327 (1993).
- [16] R. F. W. Bader, *Atoms in Molecules – A Quantum Theory* (Oxford University Press, Oxford, 1990).
- [17] K. W. Plumb, J. P. Clancy, L. J. Sandilands, V. V. Shankar, Y. F. Hu, K. S. Burch, H.-Y. Kee, and Y.-J. Kim, *Phys. Rev. B* **90**, 041112(R) (2014).
- [18] Y. Miura, Y. Yasui, M. Sato, N. Igawa, and K. Kakurai, *J. Phys. Soc. Jpn.* **76**, 033705 (2007).
- [19] C. I. Hiley, M. R. Lees, J. M. Fisher, D. Thompsett, S. Agrestini, R. I. Smith, and R. I. Walton, *Angew. Chem.* **126**, 4512 (2014).
- [20] Y. Park, J. D. Martin, and J. D. Corbett, *J. Solid State Chem.* **129**, 277 (1997).
- [21] K. Momma and F. Izumi, *J. Appl. Crystallogr.* **44**, 1272 (2011).
- [22] See Supplemental Material at <http://link.aps.org/supplemental/10.1103/PhysRevMaterials.7.054804> for SEM and optical images of the single crystal and calculated band structures.
- [23] J. Rodríguez-Carvajal, *Phys. B: Condens. Matter* **192**, 55 (1993).
- [24] P. Giannozzi, O. Andreussi, T. Brumme, O. Bunau, M. B. Nardelli, M. Calandra, R. Car, C. Cavazzoni, D. Ceresoli, M. Cococcioni *et al.*, *J. Phys.: Condens. Matter* **29**, 465901 (2017).
- [25] J. P. Perdew, K. Burke, and M. Ernzerhof, *Phys. Rev. Lett.* **77**, 3865 (1996).
- [26] P. Scherpelz, M. Govoni, I. Hamada, and G. Galli, *J. Chem. Theory Comput.* **12**, 3523 (2016).
- [27] M. Kawamura, Y. Gohda, and S. Tsuneyuki, *Phys. Rev. B* **89**, 094515 (2014).
- [28] W. Tang, E. Sanville, and G. Henkelman, *J. Phys.: Condens. Matter* **21**, 084204 (2009).
- [29] P. E. Blöchl, *Phys. Rev. B* **50**, 17953 (1994).
- [30] A. Dal Corso, *Comput. Mater. Sci.* **95**, 337 (2014).
- [31] K. A. Müller, M. Takashige, and J. G. Bednorz, *Phys. Rev. Lett.* **58**, 1143 (1987).
- [32] S. Yamanaka, K.-i. Hotehama, and H. Kawaji, *Nature (London)* **392**, 580 (1998).
- [33] K.-i. Hotehama, T. Koiwasaki, K. Umemoto, S. Yamanaka, and H. Tou, *J. Phys. Soc. Jpn.* **79**, 014707 (2010).
- [34] S. Tsuchiya, J.-I. Yamada, S. Tanda, K. Ichimura, T. Terashima, N. Kurita, K. Kodama, and S. Uji, *Phys. Rev. B* **85**, 220506(R) (2012).
- [35] N. Werthamer, E. Helfand, and P. Hohenberg, *Phys. Rev.* **147**, 295 (1966).
- [36] R. W. Henn, W. Schnelle, R. K. Kremer, and A. Simon, *Phys. Rev. Lett.* **77**, 374 (1996).
- [37] K. Ahn, R. Kremer, and A. Simon, *J. Alloys Compd.* **303-304**, 257 (2000).
- [38] M. Ryazanov, A. Simon, and H. Mattausch, *Inorg. Chem.* **45**, 10728 (2006).
- [39] B. Keimer, S. A. Kivelson, M. R. Norman, S. Uchida, and J. Zaanen, *Nature (London)* **518**, 179 (2015).
- [40] Q. Si, R. Yu, and E. Abrahams, *Nat. Rev. Mater.* **1**, 16017 (2016).
- [41] C. Berthier, P. Molinié, and D. Jérôme, *Solid State Commun.* **18**, 1393 (1976).
- [42] E. Morosan, H. W. Zandbergen, B. Dennis, J. Bos, Y. Onose, T. Klimczuk, A. Ramirez, N. Ong, and R. J. Cava, *Nat. Phys.* **2**, 544 (2006).
- [43] K. Y. Chen, N. N. Wang, Q. W. Yin, Y. H. Gu, K. Jiang, Z. J. Tu, C. S. Gong, Y. Uwatoko, J. P. Sun, H. C. Lei, J. P. Hu, and J.-G. Cheng, *Phys. Rev. Lett.* **126**, 247001 (2021).
- [44] T. C. Kobayashi, Y. Irie, J.-i. Yamaura, Z. Hiroi, and K. Murata, *J. Phys. Soc. Jpn.* **80**, 023715 (2011).
- [45] M. Zehetmayer, *Supercond. Sci. Technol.* **26**, 043001 (2013).
- [46] I. Mazin and V. Antropov, *Phys. C: Supercond.* **385**, 49 (2003).
- [47] A. P. Petrović, R. Lortz, G. Santi, C. Berthod, C. Dubois, M. Decroux, A. Demuer, A. B. Antunes, A. Paré, D. Salloum *et al.*, *Phys. Rev. Lett.* **106**, 017003 (2011).